

Direct measurement of the system-environment coupling as a tool for understanding decoherence and dynamical decoupling

Ido Almog¹, Yoav Sagi¹, Goren Gordon², Guy Bensky², Gershon Kurizki², and Nir Davidson¹
¹*Department of Physics of Complex Systems, Weizmann Institute of Science, Rehovot 76100, Israel and*
²*Department of Chemical Physics, Weizmann Institute of Science, Rehovot 76100, Israel*

Decoherence is a major obstacle to any practical implementation of quantum information processing. One of the leading strategies to reduce decoherence is dynamical decoupling — the use of an external field to average out the effect of the environment. The decoherence rate under any control field can be calculated if the spectrum of the coupling to the environment is known. We present a direct measurement of the bath coupling spectrum in an ensemble of optically trapped ultracold atoms, by applying a spectrally narrow-band control field. The measured spectrum follows a Lorentzian shape at low frequencies, but exhibits non-monotonic features at higher frequencies due to the oscillatory motion of the atoms in the trap. These features agree with our analytical models and numerical Monte-Carlo simulations of the collisional bath. From the inferred bath-coupling spectrum, we predict the performance of well-known dynamical decoupling sequences: CPMG, UDD and CDD. We then apply these sequences in experiment and compare the results to predictions, finding good agreement in the weak-coupling limit. Thus, our work establishes experimentally the validity of the overlap integral formalism, and is an important step towards the implementation of an optimal dynamical decoupling sequence for a given measured bath spectrum.

I. INTRODUCTION

In any implementation of quantum information processing by qubits [1] it is crucial to keep the qubits coherent for long periods of times. The qubits, however, are never completely isolated from the environment. This coupling to the environment means that after some time an entanglement between the system (the qubits) and the environment (all other degrees of freedom) is established. Usually the environment (bath) consists of many degrees of freedom which are not controlled. This means that one has to trace over these degrees of freedom to obtain the state of the system. The entanglement to the bath and the tracing leave the system in a separable classical state. Obviously, the resulting loss of coherence (decoherence) is one of the major obstacles towards the successful implementation of quantum information processing.

Over the years, several strategies have been suggested to cope with the decoherence problem. Clearly, the first thing to do is to minimize the coupling to the environment. Borrowing ideas from classical error correction theory, it was shown that by encoding a logical qubit in several physical qubits, it is possible to correct for errors which are introduced in the calculation process [1]. Quantum error correction protocols can correct errors up to some maximal rate. The upper bound on the error probability of a quantum gate depends on the details of the error correction protocol, but the typical values range from 10^{-4} to 10^{-2} . The gate can also be an identity gate which describes the storage of information in a quantum memory. Such a memory is essential in the architecture of a quantum network in order to enable scalability [2].

Dynamical decoupling (DD) is a technique that was developed to further reduce the error rate below the fault tolerant threshold [3–7]. The main idea of DD is to use external control fields that induce rotations of the qubit in the Bloch sphere such that the overall decoherence is

reduced. This method was first considered in the context of nuclear magnetic resonance [8–10]. In the field of quantum information processing, the pursuit for fault tolerance has pushed forward the development of a similar formalism for controlling the decoherence of noisy qubits [3, 4, 6]. The simplest example of DD is the well-known Hahn echo technique: a single population inverting pulse (π -pulse) is introduced exactly at half the final observation time [11]. The echo technique is widely used and very efficient in counteracting the effect of a quasi-static coupling to the environment. Once the coupling spectrum extends to higher frequencies, the echo technique fails and more elaborate control sequences are needed.

A strategy aimed at maximizing the decoupling has been developed by Kofman and Kurizki [12–17], based on a formula that relates the decoherence rate to the overlap of the bath coupling spectrum on the control power spectrum. This overlap can be minimized under the constraint of the available control field energy [15, 17]. In order to successfully implement this decoupling control strategy, detailed knowledge of the bath-coupling spectrum is required. In this work, we explain how to measure this spectrum, and then use it to calculate the coherence of the system after a DD sequence has been applied. The experiments we present are performed in an ensemble of ultra-cold atoms held together by a potential induced by a far-off resonance laser field. This system is used not only for demonstration purposes, but also because it can serve as a quantum memory [18–23].

Two of the most widely used physical qubits are photons and neutral atoms. Photons are easy to produce, manipulate and transport. They interact weakly with their environment and therefore can remain coherent for long travel distances. This last advantage is also their disadvantage: interactions between photons are usually very small, making the implementation of an all-optical two-qubit gate very difficult. Atoms, on the other hand,

are easy to keep in one place, and can interact strongly with other atoms and electromagnetic fields. It is therefore sensible to use atoms as “stationary qubits” for storage and manipulation and use photons as “flying qubits” that carry the information between distant sites.

One of the controlled schemes of interaction between atoms and photons is electromagnetically induced transparency (EIT) [24]. In this scheme, atoms with a lambda-shape energy structure interact with two light fields called “pump” and “probe”. The pump is usually much stronger than the probe, and is used to control the interaction strength between the probe and the atomic ensemble. Turning off the pump while the probe is propagating in the atomic ensemble leads to a conversion of the photonic excitation into the coherence between the two low-lying states of the atoms. This is sometimes called “storage of light”, although only the coherence which was carried by the light is actually stored in the ensemble. The beauty of this conversion process is that it is reversible, which makes the atomic ensemble a true memory.

In order to increase the efficiency of the storage and retrieval processes, it is desirable to work with atomic ensembles with high optical depth [25, 26]. This is because the coupling of the atoms to the external electromagnetic field scales as the square root of the number of atoms in a volume where the light intensity is approximately uniform. Working at high optical depth, however, usually implies that the atomic density is high and the rate of inter-particle collisions is large compared to the storage time. The coherence properties of the atomic ensemble are markedly changed due to elastic collisions [27]. From the point of view of a particular atom, other atoms can be regarded as the bath. The collisions with other atoms define the nature of the coupling to the bath. The three important physical quantities in the description of the collisional bath are: the collision rate, the inhomogeneous dephasing rate (i.e. the dephasing without collisions) and the harmonic confinement oscillation frequency. The spectral behavior of the collisional reservoir stems from the interplay between these quantities.

The goal of this work is to present a general method of measuring the bath-coupling spectrum, and demonstrate its usefulness in calculating the result of any control field. We start by reviewing the mathematical formalism of the overlap integral spectrum and the power spectrum of the control sequence that acts as filter function (Section II). Using this formalism it is possible to calculate from the bath-coupling spectrum the coherence at some observation time with any control sequence, as long as the so-called ‘weak coupling’ limit applies. In particular, it can be used with a null control sequence, which simply describes a dephasing process. For a known filter function of the control field, it is possible to de-convolve the overlap integral to obtain the bath-coupling spectrum. We present this technique for a constant-power continuous control field in Section III, and illustrate it by full 3D Monte-Carlo simulations. We then employ the technique to measure directly the collisional bath spectrum

in our cold atomic ensemble (Section IV). The measured bath shows interesting non-monotonic behavior due to the oscillatory motion of the atoms in the trap. Once the bath-coupling spectrum is known, it is interesting to test its implications for the outcome of other DD sequences. This is done in Section V, where we use the measured bath and the overlap-integral formalism to calculate the coherence under the well-known CPMG, UDD and CDD sequences. We then experimentally apply these DD sequences and compare the results with the predictions of the theoretical calculations based on the measured bath. We conclude and give our outlook in Section VI.

II. THE SPECTRAL OVERLAP INTEGRAL APPROACH TO THE FIDELITY CALCULATION

In this section we review the formalism [12–17] which is useful to calculate the ensemble coherence at a given time. Here we give a simplified version of this approach assuming an effective two-level stochastic Hamiltonian weakly coupled to the environment.

We consider the same model as was described in Ref. [28]. Our ensemble consists of two-level systems (TLS), and due to inhomogeneities in the external environment, the transition energy of each TLS is different than the frequency it may have in free space (we shall call this difference the detuning). We reduce the full many-body Hamiltonian to an effective single particle Hamiltonian given by

$$\hat{H} = \hbar [\omega_0 + \delta(t)] |2\rangle \langle 2| + \hbar \Omega(t) |2\rangle \langle 1| + h.c. \quad , \quad (1)$$

where ω_0 is the free space transition frequency between the two states, $\delta(t)$ is the detuning, and $\Omega(t)$ is a classical external control field which is going to be used for the DD. The detuning is a random function of time, and we assume it is averaging to 0 over different realizations of the Hamiltonian. The reduced density matrix can be calculated by

$$\rho(t) = \overline{|\phi(t)\rangle \langle \phi(t)|} \quad , \quad (2)$$

where $\phi(t)$ is the state of the system at time t with a specific realization of the stochastic Hamiltonian, and the average is taken over many realizations. $|\phi(0)\rangle$ is the initial state of the system, and ultimately our goal is to conserve this state in the ensemble for as long as possible. To characterize how well this goal is achieved it is instructive to introduce the fidelity function:

$$\mathcal{F} = \langle \phi(0) | \rho(t) | \phi(0) \rangle \quad , \quad (3)$$

which starts at 1 and decays to 0.5 at long times.

To make the model clearer, we now relate these definitions to atomic ensembles [27]. In our system, ultracold atoms are confined by an external optical potential. Although the atoms have many energy levels, we confine our attention to two low-lying states with negligible sponta-

neous decay. The potential is not exactly the same for the two states. The main source inhomogeneous broadening is that the energy difference between the two states, which is proportional to the total energy of the atom, is changing in space [29]. The phase space density of our ensemble is low enough to be considered classical (far from quantum degeneracy). The motion of the atom in the external potential causes the transition frequency to change in time. Since the ensemble consists of many atoms, each with a different trajectory, measuring the coherence of the ensemble gives the averages discussed above in a single shot. In the experiment, the coherence is measured in a time-domain Ramsey-like experiment, as described in Ref. [27].

We shall define two functions which are going to be useful later for the calculation of the fidelity. First, the bath coupling spectrum characterizes the spectral content of the coupling of the system to the bath and is defined as

$$G(f) = \int_{-\infty}^{\infty} e^{-2\pi i f \tau} \langle \delta(t) \cdot \delta(t + \tau) \rangle d\tau , \quad (4)$$

where $\langle \dots \rangle$ stands for the averaging over many realizations of $\delta(t)$. $G(f)$ is the Fourier transform of the time correlation function of $\delta(t)$. The second function we define is a 'filter function' which characterizes the power spectrum of the control sequence:

$$F_t(f) = \left| \int_0^t e^{-2\pi i f t} \cdot \cos \left(\int_0^t \Omega(\tau) d\tau \right) dt \right|^2 . \quad (5)$$

Note that although $F_t(f)$ is defined in the frequency domain, it does depend on the observation time t .

A simple expression for the fidelity at time t can be obtained under the *weak coupling* assumption, namely that the fidelity decay during the bath correlation time is negligible. In this case the fidelity is given by the overlap integral [12, 13, 15]:

$$\mathcal{F}(t) = \frac{1}{2} (1 + e^{-R(t)t}) , \quad (6)$$

where $R(t)$ is the decay rate given by the overlap integral

$$R(t) = \frac{2\alpha}{t} \int_0^t G(f) F_t(f) df , \quad (7)$$

where α is a constant between 0 and 1, depending on the assumptions for the statistics of the initial state, in particular, $\alpha = \frac{1}{4}$ for an initial state which is an equal superposition of the two internal states. Generally speaking, $R(t)$ is not constant and therefore the decay is not exponential: a signature of the non-Markov time-domain.

A related quantity is the ensemble coherence, which is defined to be the normalized off-diagonal element of the reduced density matrix [30]. In the overlap integral framework, the coherence is given by $\mathcal{C}(t) = e^{-R(t)t}$. In the Bloch sphere representation, the coherence is given by

the length of the Bloch vector, which is usually measured by quantum state tomography [1, 28].

III. HOW TO MEASURE THE BATH COUPLING SPECTRUM ?

In order for Eqs. (6-7) to be useful, one has to know the bath coupling spectrum $G(f)$, preferably from experimental data. This spectrum can be inferred from Eq. (7) by measuring the coherence for a given pulse sequence with a known $F_t(f)$. Obviously, if $F_t(f)$ were a Dirac δ function, the decay rate would be linearly proportional to the bath coupling spectrum. A good approximation to a δ function can be obtained if the control field is nearly-continuous and on-resonant field. This control field causes Rabi oscillations with a frequency f_0 which depends on its strength. The resulting filter function is a sinc-function centered around f_0 . To be more precise, the filter function is given by

$$F_t(f) = \frac{1}{4} t [\text{sinc}^2(t(f - f_0)) + \text{sinc}^2(t(f + f_0))] , \quad (8)$$

where t is the pulse duration. For this pulse, assuming $f_0 T \gg 1$, Eq. (7) yields the following decoherence rate:

$$R(f_0) \cong \frac{1}{4} G(f_0) . \quad (9)$$

We see, then, that by scanning the strength of the control fields (thus scanning f_0) and measuring the decay of coherence, it is possible to directly measure the bath coupling spectrum.

To illustrate the method and check its sensitivity to the weak-coupling assumption, we have run a 3D Monte-Carlo simulations of a cold atomic ensemble trapped in an optical potential. The simulation solves for the classical Newtonian motion of 3500 atoms. The initial conditions of the atoms are drawn from a Boltzmann distribution, assuming a temperature of $7\mu K$. As explained previously, the fluctuations in our system originate from elastic collisions between the atoms, and it is therefore necessary to include them in the simulation. In order not to run into computational complexity problems, we have developed a mean-field technique [31]. Once the trajectories of all the atoms are calculated, we calculate the energy shift of the internal states induced by the external potential along the trajectory of each atom. In our $\gamma = 1.06\mu m$ -wavelength dipole trap, the differential shift of the internal states is $6.6 \cdot 10^{-5}$ times the overall potential [29]. These energy shifts are then used to solve the Bloch equations [32] in the presence of the control field. We calculate the decoherence rate by computing the length of the Bloch vector at different times and fit it to a decaying exponent.

We simulate a measurement of the bath spectral function as described above by a continuous control field, in two parameter regimes which correspond to weak and

strong coupling. The results of the simulations are depicted in Figure 1. At low frequencies, the spectrum follows a Lorentzian curve which is expected since the fluctuations originate from a scattering process with Poisson statistics [28]. Also apparent in the spectrum is a non-monotonic feature, due to the oscillatory motion of the atoms in the trap (for more details see the next section). The only difference between the two simulations is the number of atoms, resulting in different correlation times of the bath. It is interesting to note that by increasing the number of atoms one also decreases the decoherence rate at low frequencies, a result of collisional narrowing (see Ref. [27] for more details). Thus, increasing the number of atoms increases both the collision rate and the coherence time, thereby pushing the ensemble deeper into the weak-coupling regime. Note that the relevant decoherence rate for considering whether the system is weakly coupled is the decoherence rate obtained *with* the decoupling pulse. This means that a system can be in the strong-coupling regime at low frequencies and in the weak-coupling regime at high frequencies, whence deviations from the calculated spectrum are larger at low frequencies.

IV. MEASUREMENT OF THE BATH COUPLING SPECTRUM

We have used the technique described in the previous section to measure the bath coupling spectrum in an ensemble of colliding ultra-cold atoms. In the experiment, ^{87}Rb atoms are trapped in an optical potential created by a far-off-resonance laser with a wavelength of $1.064\mu\text{m}$. Initially $\sim 10^9$ atoms are trapped and cooled in a magneto-optical trap, and further cooled by the Sisyphus [33] and Raman-sideband techniques [34]. We then use rapid adiabatic passage with a constant RF radiation and a ramped-up magnetic field to transfer the atoms from the state $|5^2S_{1/2}, F=1; m_f=1\rangle$ to the state $|5^2S_{1/2}, F=1; m_f=-1\rangle$ for $\sim 69\%$ of the atoms, and the rest to the state $|5^2S_{1/2}, F=1; m_f=0\rangle$. The thermodynamic parameters of the ensemble are measured by absorption-imaging of the cloud.

The optical trap consists of two beams crossing at an angle of 28° after passing through a zoom system capable of controlling their waist. We start by collecting the atoms in a $180\mu\text{m}$ -waist beam, and then dynamically compress the waist down to $50\mu\text{m}$. The polarization of the two crossing beams is parallel to the magnetic field, and their frequency differs by 120MHz , in order to eliminate standing waves. In this experiment we choose to work with the two states $|1\rangle = |5^2S_{1/2}, F=1; m_f=-1\rangle$ and $|2\rangle = |5^2S_{1/2}, F=2; m_f=+1\rangle$. At the applied magnetic field of 3.23 Gauss these states are Zeeman insensitive to magnetic field fluctuations to the first order [35]. The two states are separated by an energy of $2\pi\hbar \cdot 6.833\text{GHz}$, but are slightly affected by the differential AC Stark shift of the dipole trap [29]. As explained

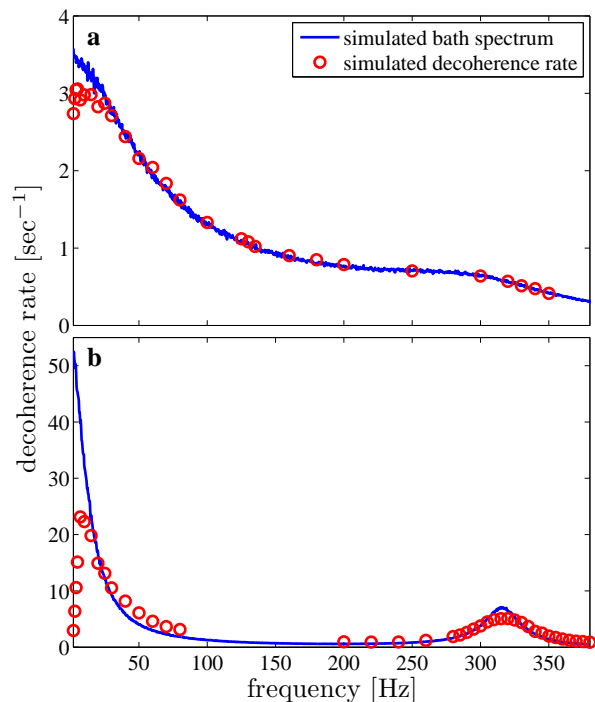


FIG. 1. Numerical simulations of the bath-coupling spectrum inferred from decoherence measurements as compared to the direct calculation. We simulate the classical motional of ^{87}Rb atoms in the trap. The blue solid line is the bath spectrum as calculated directly from the detunings along the atomic trajectories using Eq. (4). The red circles are the decoherence rates of atoms subject to a continuous field (long pulse) with the Rabi frequency plotted on the x-axis. The conditions of the simulations are a temperature of $T = 7\mu\text{K}$, radial and axial oscillation frequencies of $2\pi \cdot 600\text{Hz}$ and $2\pi \cdot 160\text{Hz}$, respectively, and number of atoms, $N = 2 \cdot 10^6$ for graph (a) and $N = 1.5 \cdot 10^5$ for graph (b). The deviation of low frequencies of the simulated decoherence measurements from the directly simulated spectrum is due to the breakdown of the weak-coupling assumption. The number of atoms is different in the two graphs and so is the frequency at which the breakdown occurs. In graph (a) the non-monotonic spectral feature (peak) is smeared due to the much larger Lorentzian width.

above, for a moving atom this shift is time-dependent and follows the trajectory.

Since $\Delta m = \pm 2$ between the two internal states, the external control $\Omega(t)$ has to be effected by a two-photon transition. We employ RF radiation at 2.15MHz and microwave radiation at 6.832527928GHz , which is chosen such that both frequencies are detuned by 90kHz from the intermediate level $|5^2S_{1/2}, F=2; m_f=0\rangle$. The maximum Rabi frequency we achieve is $\Omega = 2\pi \cdot 1000\text{Hz}$. To detect the state of the atoms we use a state-selective fluorescence-detection scheme, similar to the one described in Ref. [36].

Two main difficulties arise from driving the system by a strong control field. First, at high Rabi frequencies any inaccuracies from shot to shot in the field strength trans-

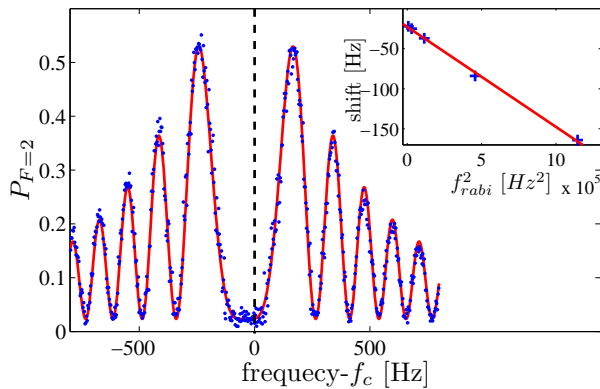


FIG. 2. Calibration of the microwave dressing effect. The y-axis shows the population at $F=2$ as a function of the control pulse frequency shifted by f_c , the center frequency without the dressing. The data was taken with a Rabi frequency of $\Omega = 340\text{Hz}$. We fit the data to the theoretical curve $A \frac{f^2}{(f-f_0)^2 + f^2} [1 + \cos(\phi + T \sqrt{(f-f_0)^2 + f^2})]$, where T is the duration of the Rabi pulse and f is the field frequency. The fit gives f_0 , the dressing for the applied Rabi frequency. In this example, the shift is -37Hz . The inset shows the microwave dressing shift as a function of the Rabi frequency squared.

late into noise in the atomic population. For example, an average noise of 1% in the Rabi frequency transforms into $\sim 100\%$ noise in the atomic population, if we drive our system at $\Omega = 2\pi \cdot 100\text{Hz}$ for 1sec. Strictly speaking, this noise in the control field results in a reduction of the fidelity. In order to avoid this difficulty, we randomize completely the initial population difference by an additional pulse that rotates the atomic state by a random uniformly distributed angle and analyze ~ 30 data points taken for the same pulse power using envelope spectroscopy. The corresponding Bloch-vector length is estimated using the maximum likelihood estimator. Since the angle of the Bloch vector is now completely random we can assume that its z-component is $C \sin(\Phi)$, where Φ is a uniformly distributed random phase. The results of the maximum-likelihood algorithm that extracts the Bloch vector length C coincide with the extreme values of the measured z-component (the population inversion).

The second difficulty is due to the energy-level shift induced by the control field [37]. This “field dressing” of the levels depends on the microwave field strength (we do not observe the shift due to the rf field). When the bath spectrum is measured using a continuous control field, this effect causes the control to have a detuning which depends on its strength (and therefore on its Rabi frequency). We measure the shift by applying a long pulse which induces Rabi oscillations and detect the population at state $|2\rangle$ while scanning the frequency of the microwave field. Such a measurement is shown in Figure 2. This data yields the relative-level shift for a given Rabi frequency. We then repeat this measurement for several Rabi frequencies and obtain a calibration graph, shown in the inset of Figure 2. As expected from theory, the

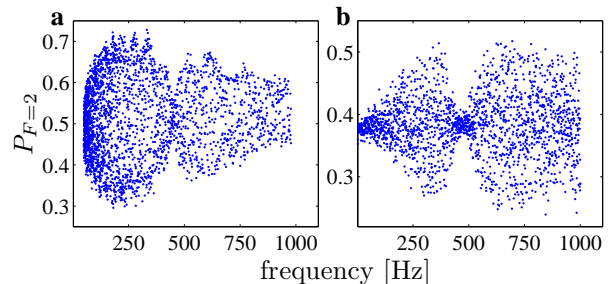


FIG. 3. Raw data of coupling spectra. The points are the population at $F=2$ as a function of the control pulse Rabi frequency. The experiment was done for 160k atoms in a trap with a radial and axial oscillation frequencies of $2\pi \cdot 910\text{Hz}$ and $2\pi \cdot 240\text{Hz}$, respectively. The field dressing results in the reduction of the contrast which is dominant in high frequency. On the right we show that after correction for this field-dressing the contrast does not decay at higher frequencies even after 1sec. The contrast between the two graphs is different since the observation time is 0.4sec for the left graph and 1sec for the right graph. The difference in the mean population stems from m-changing transitions in the $F = 2$ hyperfine level. The coherence is calculated by a maximal likelihood method (see text), and is determined by the envelope of the scattered data points.

dressing at small field strengths is linearly proportional to the control-field Rabi-frequency squared [37].

In Figure 3 two examples of raw data from a bath-spectrum measurement are shown. The scattering of the data points is a consequence of our randomization technique explained above. The bath-coupling spectrum at a given frequency is related to the envelope of the scattered points. The data presented in Figure 3a was taken without changing the control field frequency (not to be confused with its strength which controls the Rabi frequency).

The second difficulty described above leads to a substantial reduction of the contrast at higher Rabi frequencies due to the detuning of the control field from resonance, caused by the strong field-dressing of the levels. In order to eliminate this effect, we change the frequency of the microwave field as its power changes to compensate for the field dressing. The result is shown in Figure 3b to restore contrast at high frequencies. In general, this correction should also be applied in other DD sequences. In the cases we present below, however, the dressing effect is very small and unimportant.

To obtain the bath-coupling spectrum, we repeat the measurement described above with at least three different Rabi pulse durations. From each such experiment we get the coherence at that time for all Rabi frequencies. For each Rabi frequency we fit the decay of the coherence at different times to a decaying exponent, from which we obtain the decoherence rate. As explained above, the fitting to an exponent is justified in the weak-coupling regime. In Figure 4 we plot the experimentally measured decoherence rate as a function of frequency. Similarly to

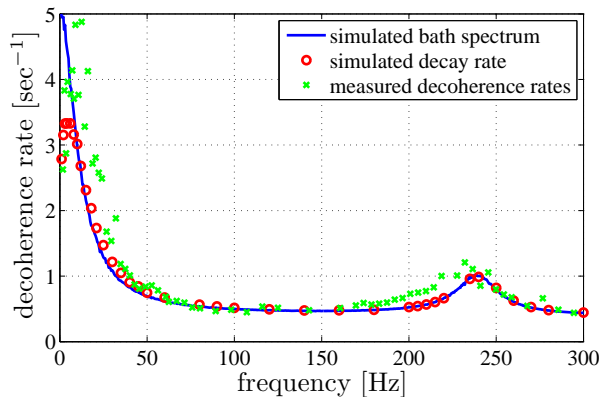


FIG. 4. Comparison of the measured bath spectrum (plus signs) to the simulated spectrum (solid line) and decoherence rate (circles). The conditions for the experiment and simulation are $340k$ atoms at a temperature of $3.5\mu K$, and with the power of the trapping laser being $1.7W$, creating a trap with a radial and axial oscillation frequencies of $2\pi \cdot 450Hz$ and $2\pi \cdot 120Hz$, respectively. The simulated spectrum was shifted by a constant of $0.4s^{-1}$ to better fit the data. This shift accounts for T_1 processes and a bias which arises due to noise in the measurements.

the simulations presented in Figure 1, the measured spectrum follows a Lorentzian at low frequencies and shows a non-monotonic feature at twice the axial oscillation frequency. This feature arises due to the rapid oscillation of the atoms in the potential. The reason is that the detuning function $\delta(t)$ always has a component at twice the oscillation frequency of the trap (since the detuning is proportional to the potential which scales as x^2). Measuring at twice this frequency couples to this component and produces higher decoherence [38].

For comparison we plot in Figure 4 the results of our Monte-Carlo simulation with the same parameters as those measured in the experiment. The agreement between the measured and simulated spectrum is quite satisfactory. We observe some shift between the two spectra in the position of the non-monotonic feature. This is probably due to small inaccuracies in the measured laser power and waist used in the simulation. The measured width of the second peak is larger in the experiment, probably due to the anharmonicity of the Gaussian confining potential which is not simulated.

Figures 1-4 prove the ability of this technique to observe small dynamical effects through the spectrum. We note that although other methods to measure the oscillation frequency of the trapping potential exist, the use of the spectrum to infer this quantity is unique in that it does not require excitations of the atoms.

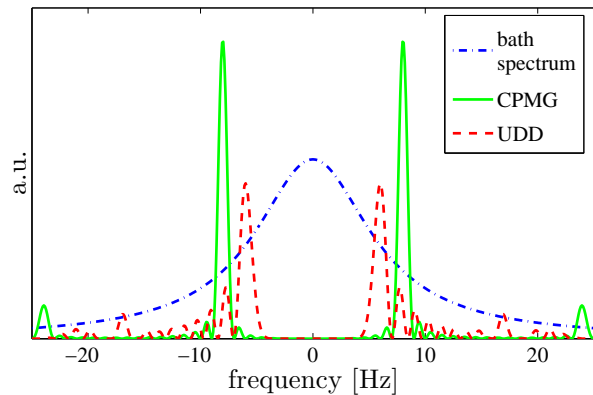


FIG. 5. The collisional bath-coupling spectrum, the filter functions and their overlap, calculated from the formula (Eq. (7)) for two DD sequences: CPMG and UDD. The dash-dotted line is a Lorentzian spectrum which describes the Poisson statistics of elastic collisions. The filter function for the CPMG decoupling sequence (solid line) and UDD (dotted line), both consisting of 16 π -pulses for an observation time of 1sec. The UDD spectral overlap is larger at lower frequencies compared to the that of CPMG. Since the bath-coupling spectrum at these frequencies is higher (which means a faster decay), the resulting decoherence rate for UDD is larger than for CPMG.

V. DYNAMICAL DECOUPLING AND THE BATH SPECTRUM

As explained in Section II, the bath coupling spectrum is most useful for calculating the outcome of any DD sequence. In general, for a given bath spectrum and a set of constraints (such as the maximum duration, energy or action of the control pulse), it is possible to devise an optimal decoupling sequence [17, 39]. There are, however, well-known sequences which are suitable for certain classes of noise spectra. Here we concentrate on three such sequences: the Carr-Purcell-Meiboom-Gill sequence (CPMG) [40–42], the concatenated DD sequence (CDD) [6], and the sequence developed by Uhrig (UDD) [7]. Although in this work we restrict ourselves to sequences of brief π -pulses, this is not required by the theory. To compare the performance of the three sequences we consider the decoherence they yield for a given number of π pulses.

In Figure 5 we depict schematically the Lorentzian spectrum of our collisional bath and the filter function (Eqs. (7)-(9)) of the CPMG and UDD sequences with 16 π pulses. The CPMG spectrum has a sharp peak at $f_0 = 8Hz$, half the pulse rate, and smaller peaks at lower and higher frequencies whose envelope is proportional to $1/(f - f_0)^2$. There are also peaks at harmonies centered around $3f_0$ but their area is 9-times smaller than that of the main peak. UDD has exponentially reduced coupling at low frequencies. This can be very useful for bath spectra which have a cutoff at high frequencies [43], which is not the case of the Lorentzian spectrum. Namely,

the UDD exponential suppression of the lower sidebands, comes with a price: for the same number of pulses the maximum coupling is at lower frequency, hence for many physical coupling spectra, including Lorentzian spectra, it will sample portions of the spectrum with larger decoherence. CDD (not shown in the graph) has similar properties to UDD. It has an exponentially reduced coupling in part of the spectrum, but its overlap with a Lorentzian is overall the same.

Experimentally, we apply the DD sequences for a duration of 0.4sec, on an ensemble prepared with the same conditions as in the previous section. The atoms are initialized to an equal superposition $|\Psi\rangle = |1\rangle + |2\rangle$, which we want to preserve. The duration of a π -pulse was chosen in these experiments to be 2.3msec, corresponding to a maximal Rabi frequency of 217Hz. To reduce the noise introduced by the inaccuracies in the control field, we switch the phase of the control by a π -phase every two pulses $\pi, \pi, -\pi, -\pi, \dots$ [28]. The final atomic state at the end of the sequence is determined using state tomography. Our measurement of the population gives only the z-component of the Bloch vector. In order to measure the other two components we apply before the measurement an additional $\pi/2$ rotation around the x or y axes. We tune the duration of our π pulses in the DD sequences such that there is only a small z-component after the sequence. The x and y components are measured by a Ramsey technique, in which we vary the phase of a final $\pi/2$ pulse and measure the contrast of the fringe. In other words, the state tomography gives us the ability to tune correctly the π pulse duration such that the final state always resides in the equatorial plane of the Bloch sphere. It is then more accurate to measure the coherence by applying a final $\pi/2$ pulse with a controlled phase and detect the population in the z-axis. Finally, we calculate the coherence time by fitting the decay of the fringe contrast at different times to a decaying exponent.

The results of these measurements are presented in Figure 6. For all DD sequences the coherence time increases as the number of pulses grows. As expected from the overlap between the filter functions of the DD sequences and the bath spectrum (see Figure 5), the CPMG surpasses both UDD and CDD, which in turn behave quite similarly. We stress that our ranking between the DD sequences is only valid for our experimental collisional bath. Even more interesting than the relative performance of the DD sequences is to compare them with the theory presented in Section II. To this end, we take the measured bath spectrum from the previous section (Figure 4) and use it in the overlap integral formalism to calculate the predicted outcome of each sequence. There is, however, a depopulation T_1 process in our system which results from m-changing transitions in the F=2 hyperfine level. We measure this timescale directly to be $T_1 = 2.2$ sec in our experimental conditions. Since the T_1 and T_2 processes are not correlated, the total decay is the sum of the decay rates of both processes. In practice, we subtract from the measured bath spectrum the bias

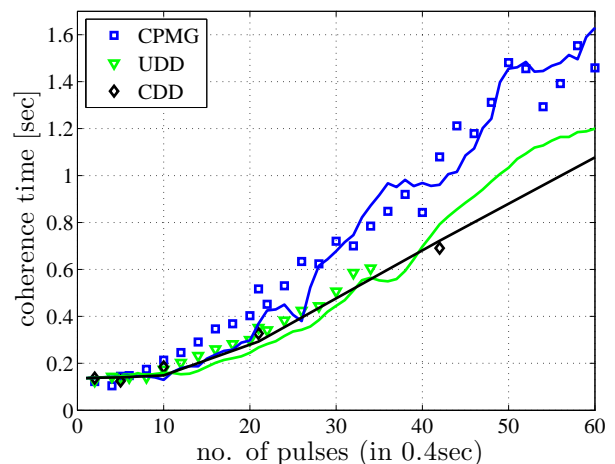


FIG. 6. Coherence times under different DD pulse sequences. We compare the sequences CPMG (blue squares), UDD (green triangles) and CDD (black diamonds) for a given number of pulses at an observation time of 0.4sec. The performance of both UDD and CDD is worse than the CPMG, as expected from their overlap with the bath spectrum (see Figure 5). The solid line is the coherence time as calculated based on the overlap integral of the sequences filter functions with the measured bath spectrum. The conditions of the ensemble are the same as for the measured bath spectrum in the previous section. Note that the CDD sequence cannot have any number of pulses, and this is the reason why there are only 5 data points for this sequence.

which results from the T_1 process and the noise in the measurement. By doing so we can calculate only the decoherence resulting due to the fluctuations of $\delta(t)$ (the T_2 process decoherence rate). We then add to it the decay due to the T_1 process, which is given by $2/T_1$. The total decoherence rate is depicted as a solid line in Figure 6, and agrees very well with the coherence times that were measured directly. We attribute the small deviations at low frequencies to a departure from the weak-coupling regime.

VI. CONCLUSIONS AND OUTLOOK

To summarize, we have presented a method of measuring directly the bath-coupling spectrum, and used it for optically trapped ultracold atoms. The measured spectrum follows a Lorentzian shape at low frequencies, which is expected, since the source of fluctuations is s-wave scattering between the atoms [28]. At higher frequencies, though, the spectrum exhibits non-monotonic features which arise due to the rapid oscillatory motion of the atoms in the trap. The usefulness of the concept of the bath-coupling spectrum is tested by its ability to predict the outcome of any DD control sequence. We have measured directly the performance of three well-known sequences: CPMG, UDD and CDD. The comparison of

these measurements to a calculation based on the overlap integral with the directly measured bath spectrum proves the validity of this framework at the weak-coupling limit. As was already shown numerically in [28], the CPMG sequence is found to be superior to the UDD and CDD sequences, for our collisional bath spectrum.

As noted above, the weak-coupling assumption is essential for the overlap-integral formalism to be correct. Under certain experimental conditions and at low frequencies, our bath does not fulfil this assumption, and indeed we observe deviations from the corresponding theoretical calculations. Measuring the coupling spectrum under these conditions is a major challenge. One way of addressing it is by using a sequence that mostly resides in the weak-coupling part of the spectrum, while a small sideband probes the low frequencies of the spectrum. The idea is to keep most of the overlap between the spectrum and the filter function in the weak-coupling domain, while still probing the strong coupling domain of the spectrum. An example of such a pulse is:

$$\Omega(t) = 2\pi f_0 \left(1 + \beta \frac{f_m}{f_0} \cos(2\pi f_m t)\right), \quad (10)$$

where f_0 is the carrier Rabi frequency, β is the modu-

lation index and f_m is the AM modulation frequency. By measuring the decoherence twice: once with the sideband and once without, it is possible to extract the coupling spectrum at the sideband frequency, even if this frequency is in the strong-coupling part of the spectrum.

For a given bath spectrum and a set of constraints on the control field, an optimal decoupling sequence can be constructed [17, 39]. This is done by solving the Euler-Lagrange equation which minimizes the overlap of the control-field filter function and the bath-coupling spectrum. This procedure is yet to be demonstrated experimentally. In our system, as well as in other systems, the spectrum is non-monotonic and as such we expect a non-trivial optimal decoupling sequence. What can complicate this picture is noise in the control field. In this work we have circumvented this issue by using an envelope spectroscopy method. It is possible to extend the overlap-integral formalism to include the classical noisy control as a second (classical) bath-like spectral function. The decay rate is then given by two overlap integrals which can be solved to find the optimal DD sequence for a noisy control. Since noise in the control is always present, this extension of the theory is both necessary and practical.

We acknowledge the financial support of MIDAS, MINERVA, GIF, ISF, and DIP.

-
- [1] Nielsen, M. A. and Chuang, I. L. *Quantum Computation and Quantum Information*. Cambridge University Press, (2000).
 - [2] Duan, L. M., Lukin, M. D., Cirac, J. I., and Zoller, P. *Nature* **414**, 413 (2001).
 - [3] Viola, L. and Lloyd, S. *Phys. Rev. A* **58**, 2733 Oct (1998).
 - [4] Viola, L., Knill, E., and Lloyd, S. *Phys. Rev. Lett.* **82**, 2417 (1999).
 - [5] Search, C. and Berman, P. R. *Phys. Rev. Lett.* **85**, 2272 (2000).
 - [6] Khodjasteh, K. and Lidar, D. A. *Phys. Rev. Lett.* **95**, 180501 (2005).
 - [7] Uhrig, G. S. *Phys. Rev. Lett.* **98**, 100504 (2007).
 - [8] Kubo, R. *Fluctuation, relaxation and resonance in magnetic systems*, 23. Scottish Universities Summer School in Physics. Oliver and Boyd, Edinburgh and London (1961).
 - [9] Kubo, R. *J. Phys. Soc. Jpn.* **9**, 935 (1954).
 - [10] Haeberlen, U. *High Resolution NMR in Solids*. Advances in Magnetic Resonance Series. Academic, (1976).
 - [11] Hahn, E. L. *Phys. Rev.* **80**, 580 (1950).
 - [12] Kofman, A. G. and Kurizki, G. *Phys. Rev. Lett.* **87**, 270405 (2001).
 - [13] Kofman, A. G. and Kurizki, G. *Phys. Rev. Lett.* **93**, 130406 (2004).
 - [14] Gordon, G. and Kurizki, G. *Phys. Rev. A* **76**, 042310 (2007).
 - [15] Gordon, G., Erez, N., and Kurizki, G. *J. Phys. B* **40**, S75 (2007).
 - [16] Gordon, G. and Kurizki, G. *Phys. Rev. Lett.* **97**, 110503 (2006).
 - [17] Clausen, J., Bensky, G., and Kurizki, G. *Phys. Rev. Lett.* **104**, 040401 (2010).
 - [18] Kuzmich, A., Bowen, W. P., Boozer, A. D., Boca, A., Chou, C. W., Duan, L. M., and Kimble, H. J. *Nature* **423**, 731 (2003).
 - [19] Chou, C. W., de Riedmatten, H., Felinto, D., Polyakov, S. V., van Enk, S. J., and Kimble, H. J. *Nature* **438**, 828 (2005).
 - [20] Yuan, Z.-S., Chen, Y.-A., Zhao, B., Chen, S., Schmiedmayer, J., and Pan, J.-W. *Nature* **454**, 1098 (2008).
 - [21] Zhao, B., Chen, Y. A., Bao, X. H., Strassel, T., Chuu, C. S., Jin, X. M., Schmiedmayer, J., Yuan, Z. S., Chen, S., and Pan, J. W. *Nature Phys.* **5**, 95 (2009).
 - [22] Schnorrberger, U., Thompson, J. D., Trotzky, S., Pugatch, R., Davidson, N., Kuhr, S., and Bloch, I. *Phys. Rev. Lett.* **103**, 033003 (2009).
 - [23] Zhang, R., Garner, S. R., and Hau, L. V. *Phys. Rev. Lett.* **103**, 233602 (2009).
 - [24] Lukin, M. D. *Rev. Mod. Phys.* **75**, 457 (2003).
 - [25] Harris, S. E. and Hau, L. V. *Phys. Rev. Lett.* **82**, 4611 (1999).
 - [26] Gorshkov, A. V., André, A., Fleischhauer, M., Sørensen, A. S., and Lukin, M. D. *Phys. Rev. Lett.* **98**, 123601 (2007).
 - [27] Sagi, Y., Almog, I., and Davidson, N. *Phys. Rev. Lett.* **105**, 093001 (2010).
 - [28] Sagi, Y., Almog, I., and Davidson, N. *Phys. Rev. Lett.* **105**, 053201 (2010).
 - [29] Kuhr, S., Alt, W., Schrader, D., Dotsenko, I., Miroshnychenko, Y., Rauschenbeutel, A., and Meschede, D. *Phys. Rev. A* **72**, 023406 (2005).
 - [30] Cywiński, L., Lutchny, R. M., Nave, C. P., and Sarma,

- S. D. *Phys. Rev. B* **77**, 174509 (2008).
- [31] Collisions are simulated by assuming a steady state density profile and calculating each atom's local probability to undergo a collision. Once a collision occurred, we need to calculate the velocity of the atoms resulting from it. To that end we assume a virtual counterpart only for the purposes of this specific collision. The velocity of the virtual counterpart is drawn from a Maxwell-Boltzmann distribution modified relative to the velocity of the main atom (the one which is really part of the simulation). The collision itself is described in these low temperature regime by an s-wave scattering process with scattering length of $a=5.2\text{nm}$ for ^{87}Rb . We disregard the virtual counterpart after the collision. Of course, this process has to be proved self-consistent such that it reproduces the Boltzman distribution after many such collisions.
- [32] L. Allen, J. H. E. *Optical Resonance and Two-Level Atoms*. Dover Publications, (1987).
- [33] Castin, Y., Dalibard, J., and Cohen-Tannoudji, C. *Light induced kinetic effects on atoms, ions, and molecules*, chapter The limits of Sisyphus cooling. ETS Editrice (1991).
- [34] Kerman, A. J., Vuletić, V., Chin, C., and Chu, S. *Phys. Rev. Lett.* **84**, 439 (2000).
- [35] Harber, D. M., Lewandowski, H. J., McGuirk, J. M., and Cornell, E. A. *Phys. Rev. A* **66**, 053616 (2002).
- [36] Khaykovich, L., Friedman, N., Balushev, S., Fathi, D., and Davidson, N. *Europhys. Lett.* **50**, 454 (2000).
- [37] Haroche, S., Cohen-Tannoudji, C., Audoin, C., and Schermann, J. P. *Phys. Rev. Lett.* **24**, 861 (1970).
- [38] Kotler, S., Akerman, N., Glickman, Y., Keselman, A., and Ozeri, R. *arXiv:1101.4885* (2011).
- [39] Gordon, G., Kurizki, G., and Lidar, D. A. *Phys. Rev. Lett.* **101**, 010403 (2008).
- [40] Carr, H. Y. and Purcell, E. M. *Phys. Rev.* **94**, 630 (1954).
- [41] Meiboom, S. and Gill, D. *Rev. Sci. Instrum.* **29**, 688 (1958).
- [42] Vandersypen, L. M. K. and Chuang, I. L. *Rev. Mod. Phys.* **76**, 1037 (2005).
- [43] Biercuk, M. J., Uys, H., VanDevender, A. P., Shiga, N., Itano, W. M., and Bollinger, J. J. *Nature* **458**, 996 (2009).